First-principles simulations of liquid silica: Structural and dynamical behavior at high pressure

Bijaya B. Karki,[1,2] Dipesh Bhattarai,[1] and Lars Stixrude[3]
[1]*Department of Computer Science, Louisiana State University, Baton Rouge, Louisiana 70803, USA*
[2]*Department of Geology and Geophysics, Louisiana State University, Baton Rouge, Louisiana 70803, USA*
[3]*Department of Geological Sciences, University of Michigan, Ann Arbor, Michigan 48109, USA*
(Received 7 April 2007; revised manuscript received 25 July 2007; published 24 September 2007)

We have carried out first-principles molecular dynamics simulations of silica liquid over a wide range of pressure (from 0 to ~150 GPa) and temperature (3000–6000 K) within density functional theory and the pseudopotential approximation. Our results show that the liquid structure is highly sensitive to compression: the average Si-O coordination number increases from 4 at zero pressure initially slowly on compression and then more rapidly after 30% compression, reaching 6.5 at 150 GPa. At low compression, nearly all Si-O coordination environments are fourfold and relatively undistorted, whereas at high compression several coordination types (five-, six-, and sevenfold) coexist and the polyhedra are significantly distorted. The heat capacity and Grüneisen parameter show little variation with compression within the low-pressure regime and vary rapidly with compression in the high-pressure regime. Results are successfully fitted to the Mie-Grüneisen equation of state and show no evidence of spinodal instability or a temperature of maximum density. The behavior of the self-diffusion coefficient is consistent with a crossover from strong to fragile liquid behavior with increasing temperature and increasing pressure. Both Si and O self-diffusion coefficients vary anomalously at 4000 K—they initially increase with pressure and then decrease upon further compression. This anomalous behavior is absent at higher temperatures.

DOI: 10.1103/PhysRevB.76.104205 PACS number(s): 61.20.Ja, 65.20.+w, 91.60.−x, 62.50.+p

I. INTRODUCTION

Silica is one of the most widely studied materials due to its great importance in earth science and materials science. Silica is a prototype liquid: understanding the physics of this liquid is expected to lend considerable insight into the behavior of the so-called tetrahedral liquids including water,[1–4] BeF_2,[5] and $GeSe_2$.[6,7] Such liquids are known to have many interesting properties such as density minima and/or maxima, dynamical anomalies, and liquid-to-liquid phase transitions.[8–13] Liquid silica is one of the major components of geophysically relevant melts (magmas). Partial melts are believed to exist in Earth at depths as great as the core-mantle boundary (136 GPa, 2890 km depth).[14,15] Knowledge of the physical properties of liquid silica under extreme pressure and temperature conditions of the deep interior is essential to modeling the thermal, chemical, and dynamical states of the early Earth.[16,17] The equation of state of the liquid controls the relative density of partial melts produced by geological processes and coexisting solids, and thus whether these melts will rise or sink. The diffusivity controls the mobility and rate of chemical reaction of liquids with their surroundings. While there exist several experimental studies of the density,[18–22] and structural[23–30] and dynamical quantities[31–33] of primarily amorphous silica and also liquid silica at low pressures, such studies have not been performed at pressures greater than 40 GPa.

It is of fundamental interest to explore how the structure of the liquid phase changes with increasing pressure and compares with the structure of the solid phase. The high-pressure equation of state of silicate liquids, their relative density with respect to coexisting solids, and their mobility can be understood on the basis of their structure. Previous theoretical[34–40] and experimental[23–30] studies have found that amorphous silicates undergo remarkable pressure-induced changes in structure. These include a gradual pressure-induced increase in the Si-O coordination number, from fourfold at ambient pressure toward sixfold at higher pressure. Such a structural change mirrors that associated with polymorphic phase transitions in crystalline phase. However, the nature of this coordination change in the amorphous state is still poorly constrained. In particular, the mean pressure at which it occurs, the pressure range over which it takes place, and whether fourfold and sixfold coordinated states are energetically preferred and stable over finite pressure intervals are not known.[42] The structure within the transition interval is also of considerable interest: do four- and sixfold coordination states coexist over a wide range of pressure or are intermediate states (i.e., fivefold coordination) also important?[41] The presence of fivefold coordination states has been predicted to enhance mobility (self-diffusion) substantially. From the theoretical point of view, one of the uncertainties in previous studies,[9–13,34–40] which have mostly been based on semiempirical force fields, is the form of the force field chosen: various models that have been applied to amorphous silica yield significantly different results for the high-pressure structure and compression mechanisms.[42] Previous first-principles molecular dynamics (FPMD) simulations have focused primarily on low pressures,[43–46] and in one case explored compression mechanisms up to 27 GPa.[45] Spinodal instability, the temperature of maximum density, liquid-liquid phase transitions, and anomalies in the dependence of the self-diffusion coefficient on pressure and temperature, all predicted on the basis of semiempirical force fields,[9–13,38,41] have not yet been examined with first-principles methods.

In this paper, we perform FPMD computer simulations of the liquid state of SiO_2 as a function of pressure up to 150 GPa and temperature from 3000 to 6000 K to investi-

gate its structural and dynamical properties. The organization of the paper is as follows: Section II presents the computational details. Section III presents the calculated results with analysis of the equation of state, thermodynamic properties, geometric structure, and dynamical properties. Section IV discusses implications of our results and draws some conclusions.

II. METHODOLOGY

The computations have been performed using the first-principles molecular dynamics method (VASP parallel code)[47,48] as in our recent studies of liquid MgO and $MgSiO_3$.[14,49,50] The interatomic forces are computed at each time step from a fully self-consistent solution of the electronic structure to the Born-Oppenheimer surface, within the finite temperature formulation of density functional theory.[51] The local density approximation (LDA) is used[52] as this has been found to yield superior agreement with the equation of state, structure, and elasticity of silicates and oxides,[53] although we also perform a limited number of computations with the generalized gradient approximation (GGA)[54] for comparison. Ultrasoft Si (0.82 Å and $3s^2 3p^4$) and O (0.82 Å and $2s^2 2p^4$) pseudopotentials[47] are used with a plane wave cutoff of 400 eV and gamma point sampling. The Pulay correction,[55] which varies with compression from 2.8 to 6.4 GPa over the volume range considered in this study, is added to the calculated total pressure. To correct for the well-known overbinding tendency of LDA, we follow previous work[14,56,57] by adding a uniform correction to the pressure of 1.5 GPa, evaluated on the basis of comparison between the LDA equation of state of quartz to experimental data.

Our FPMD simulations are based on the canonical (NVT) ensemble in which the number of atoms in the periodically repeated unit cell (N), the volume (V), and the temperature (T) are fixed.[58] The simulation box contains 24 SiO_2 units (72 atoms). A series of FPMD simulations of the liquid state have been performed covering seven volumes: $V/V_X=1.0$, 0.9, 0.8, 0.7, 0.6, 0.5, and 0.4 along four isotherms, 3000, 4000, 5000, and 6000 K. Here, $V_X=45.80$ Å^3/SiO_2 is the reference volume, similar to the experimental volume of the liquid at the ambient melting point.[21] The corresponding pressure-temperature conditions span the freezing curve as estimated on the basis of shock-wave compression: 2000 K at zero pressure to approximately 4500 K at 150 GPa (Ref. 59) and so include the liquid stability field and also the high-pressure supercooled regime. The simulation schedule is as follows: The crystalline structure at each volume is first melted and equilibrated at 10 000 K for a period of 3 ps. A time step of 1 fs is used. We then quench the system to a desired lower temperature. At this temperature, we run the simulation long enough to reach the diffusional regime in which the mean-square displacement (MSD) of atoms varies linearly with time (see Sec. III C). We confirm that the system at each V-T condition simulated is in the liquid state by analysis of the radial distribution function as well as the mean-square displacement. For instance, at $V/V_X=1.0$ (the reference volume), simulation time periods of 3, 7, 20, and 58 ps, respectively, are required at 6000, 5000, 4000, and 3000 K. Our simulation time periods far exceed previous FPMD simulation durations of 8 ps at 3500 K from Ref. 43, 2 ps at 3500 K from Ref. 45, and 12.5 ps at 3500 K and 22.5 ps at 3000 K from Ref. 46. In our simulations, the mean displacement of the atoms from initial to final configurations is 2 Å at 3000 K and more than 5 Å at higher temperatures. Uncertainties in the energy and pressure are computed using the proper statistics via the blocking method.[60] The convergence of the time-averaged properties and systematic energy drift are tested as in our previous study of liquid MgO.[49] We find that equilibrium properties (e.g., structure, pressure, energy) converge much more quickly (i.e., within a few picoseconds at all temperatures) as in previous FPMD studies[43–46] than dynamical properties (e.g., diffusion coefficient). Previous MD studies have not predicted any significant effects of finite size on equilibrium properties or structure of silica liquid. However, this is not true in the case of its dynamical properties, and we make a critical assessment of the potential uncertainties in our calculations (see the Sec. III C).

III. RESULTS AND ANALYSIS

A. Structural properties

The radial distribution function (RDF), $g(r)$, is computed to examine the structural properties of the simulated liquid system. Figure 1 shows the partial (both like and unlike) radial distribution functions $g_{\text{Si-O}}(r)$, $g_{\text{Si-Si}}(r)$, and $g_{\text{O-O}}(r)$ at four different compression and temperature conditions, which are denoted as V1T1 ($V=1.0V_X$ and $T=3000$ K), V2T2 ($V=0.8V_X$ and $T=4000$ K), V3T3 ($V=0.6V_X$ and $T=5000$ K), and V4T4 ($V=0.4V_X$ and $T=6000$ K). These V-T points are chosen to lie uniformly 1000 K above the silica freezing curve over the compression range considered here. The size of the fluctuations after the first peak in each case decreases rapidly with distance and the RDF approaches unity at larger distances, indicating the short-range order and long-range disorder characteristic of the liquid state. The positions of the peaks at low compression agree well with experimental data on silica melt and glass as does the asymmetry in the second Si-O peak[23,61] (see Table I). For all RDFs, with increasing temperature and compression, both the first and second peaks decrease in amplitude and become broader (Fig. 1). The positions of both peaks tend to shift to smaller distances except the second peak in the Si-Si RDF, which eventually disappears at high compression and instead a new second peak appears at a larger distance (at condition V4T4). After the first peak, the like (Si-Si and O-O) radial distribution functions are very similar to each other at V1T1 and V2T2. This behavior has been seen in previous molecular dynamics simulations[38] and is remarkable because it is typical of symmetrical ionic liquids such as the alkali halides. However, at higher compression (V3T3 and V4T4), the like distributions begin to differ significantly.

The structure of the liquid demonstrates that it compresses via mechanisms that are entirely different from those operative in the crystalline polymorphs. We calculate the average Si-O, O-O, and Si-Si distances as (Fig. 2)

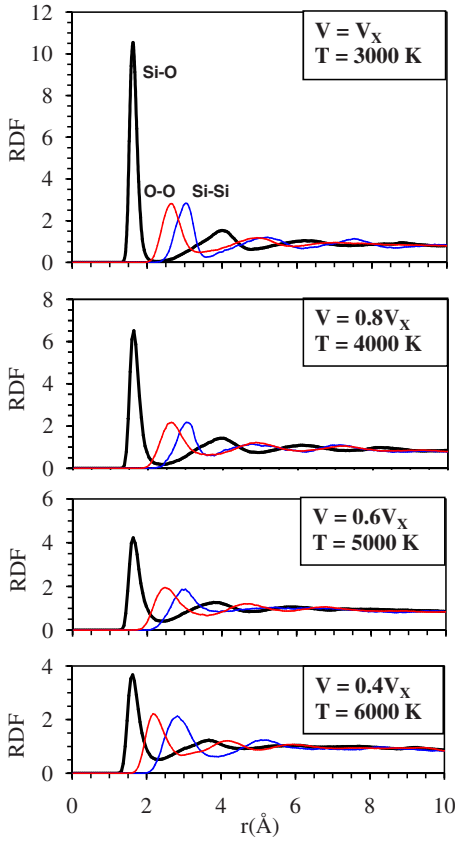

FIG. 1. (Color online) Partial radial distribution functions (RDFs) for Si-O (black), Si-Si (blue), and O-O (red) atomic pairs at condition V1T1, V2T2, V3T3, and V4T4.

$$\langle r \rangle = \frac{\int_0^{r_{\min}} r g_{\alpha\beta}(r) dr}{\int_0^{r_{\min}} g_{\alpha\beta}(r) dr}, \tag{1}$$

where $r_{\min}$ is the position of the first minimum in the corresponding $g_{\alpha\beta}(r)$. Remarkably, all three average distances gradually increase in the liquid up to 30% compression. This is in contrast to the behavior of tetrahedrally coordinated

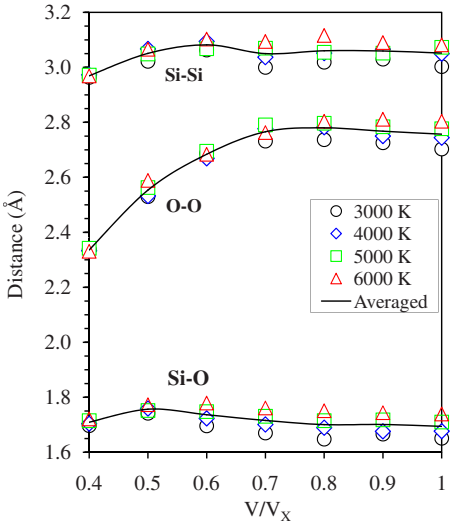

FIG. 2. (Color online) Average Si-O, Si-Si, and O-O distances as a function of compression and temperature. Lines represent the temperature-averaged distances.

crystalline phases of silica, which are stable over a similar range of volumes, and which compress almost entirely by shortening Si-Si distances. At V/V_X=0.7, O-O distances begin to decrease rapidly, while Si-Si and Si-O distances continue to increase, before finally beginning to decrease at V/V_X=0.6 and V/V_X=0.5, respectively.

We calculate the average coordination numbers (Fig. 3) via

$$C_{\alpha\beta} = 4\pi\rho x_\beta \int_0^{r_{\min}} r^2 g_{\alpha\beta}(r) dr, \tag{2}$$

where ρ is the number density and x_β is the concentration (N_β/N) of species β. The calculated Si-O, Si-Si, and O-O coordination numbers at V1T1 are, respectively, 4.02, 4.13, and 7.54, compared to the corresponding experimental values of 3.9, 3.8, and 5.7 for silica melt (Table I) and corresponding values of 4, 4, and 6 for the ambient pressure crystalline polymorph. The Si-O coordination number increases on compression, as expected by analogy with the crystalline polymorphs, but much more slowly initially than in $MgSiO_3$

TABLE I. The calculated positions of the first peak, the minimum after the first peak, and the second peak for Si-O, O-O, and Si-Si RDFs, and the corresponding coordination numbers at four *V-T* conditions. The experimental results for vitreous (Ref. 23) and liquid (Ref. 61) silica at ambient pressure are shown.

	Si-O				O-O				Si-Si			
	R_{P1}	R_M	R_{P2}	CN	R_{P1}	R_M	R_{P2}	CN	R_{P1}	R_M	R_{P2}	CN
V1T1	1.625	2.225	4.025	4.03	2.625	3.425	4.925	7.57	3.025	3.575	5.225	4.14
V2T2	1.625	2.375	3.925	4.21	2.625	3.425	4.875	10.59	3.025	3.575	4.775	5.01
V3T3	1.625	2.425	3.775	5.06	2.475	3.425	4.625	13.47	2.925	3.925	5.175	7.90
V4T4	1.625	2.375	3.675	6.52	2.175	2.925	4.175	12.17	2.825	3.725	5.175	13.03
Ref. 23	1.62		4.15		2.6		4.95		3.08		5.18	
Ref. 61	1.62		~4.2	3.9	2.65		~5	5.7	3.12		~5	3.8

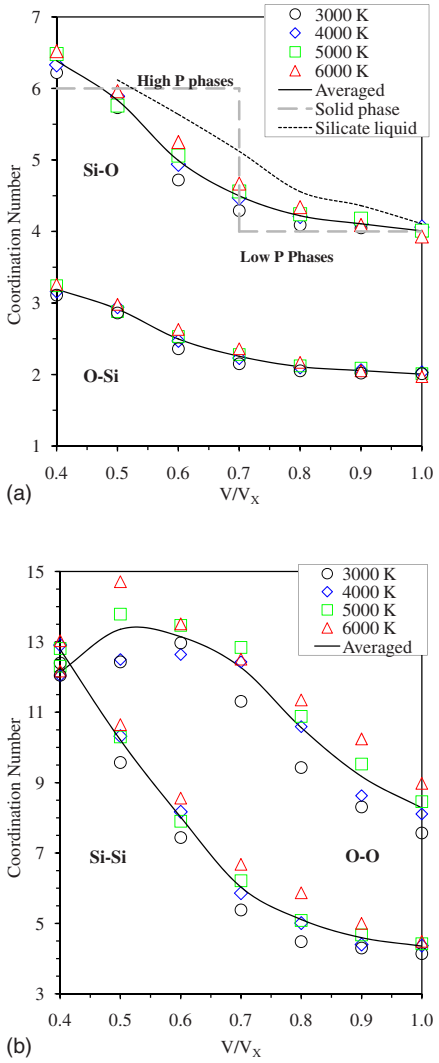

FIG. 3. (Color online) The calculated Si-O, O-Si, Si-Si, and O-O coordination numbers as a function of compression at four different temperatures. Solid lines represent the temperature-averaged values. Long dashed line represents crystalline silica phases. Short dashed line represents $MgSiO_3$ liquid (Ref. 14).

liquid (Fig. 3, top). In contrast to the silicate liquid, in which the coordination number depends nearly linearly on compression, in silica the coordination number remains very nearly 4 until V/V_X=0.8 where it begins to increase more rapidly. This behavior is consistent with the behavior of sodium-silicate glasses for which it is found that the pressure-induced Si-O coordination increase occurs more readily (at a lower pressure) in less siliceous compositions.[63] The interpretation of these results is also consistent with our findings, namely, that the Si-O coordination number increases initially at the expense of nonbridging oxygen (nominally absent in the pure silica compositions of our study).[62,64] A similar behavior (initial slow increase) with compression of O-Si coordination in silica liquid is also predicted by our calculations (Fig. 3, top). On the other hand, the O-O (and Si-Si) coordination number increases rapidly with compression and is close to 12 at the highest compression of our study, i.e., that of close-packed structures (Fig. 3, bottom).

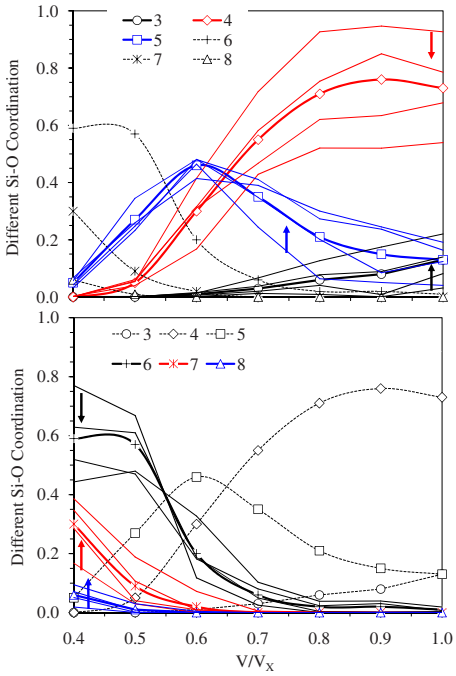

FIG. 4. (Color online) The calculated Si-O coordination numbers of different types (from three- to eightfold coordination) as a function of compression at four different temperatures (thin solid lines). Thick solid lines and dashed lines represent the temperature-averaged values of different contributions. Arrows indicate the directions of increasing temperature.

The Si-Si coordination number, however, continues to increase with compression even at the highest pressure of our study, indicating that it is not accurate to characterize further compression of the liquid simply in terms of close-packed structures.

At each volume-temperature condition, a variety of local Si-O coordination environments exist (Fig. 4). We calculate the relative proportions of different Si-O coordinations, which vary from threefold to eightfold. At low compression, fourfold coordination is dominant with noticeable contributions from three- and fivefold coordination. The proportions of these odd coordination environments decrease with decreasing temperature in the simulations (Fig. 4, top), consistent with the experimental observation that they are essentially absent in the nearly perfectly tetrahedral room temperature glass.[23,25] With increasing compression, contributions from five- and sixfold coordination increase, whereas those from three- and fourfold coordination decrease. The preponderance of fivefold Si-O coordination environments at midcompression (V/V_X=0.6) is significant for two reasons. First, it demonstrates that liquid structure is not merely a disordered version of the structure of the crystalline polymorphs, fivefold coordination being extremely rare in crystalline silicates. Second, fivefold coordination has been suggested as a particularly unstable transition state that enhances diffusion.[41] At high compression, sixfold coordination is dominant with its contribution increasing with decreasing temperature at the expenses of five- and sevenfold coordination (Fig. 4, bottom). Our results are consistent with the pre-

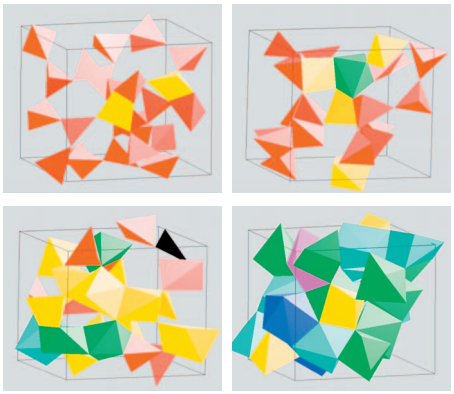

FIG. 5. (Color) Visualization of the Si-O coordination environment using the color-coded polyhedral representation at condition V1T1 (top left), V2T2 (top right), V3T3 (bottom left), and V4T4 (bottom right). The black, red, yellow, green, cyan, blue, magenta, and white colors represent the local coordination numbers of $\leqslant 3$, 4, 5, 6, 7, 8, 9, and $\geqslant 10$, respectively. The bond length is defined by the first minimum in the Si-O radial distribution function.

vious FPMD study that considered pressures up to 27 GPa.[45] For instance, at $V/V_X=0.8$ and 3500 K, we find proportions of four- (together with threefold), five-, and sixfold coordination of 87%, 13%, and 0%, respectively, compared to the corresponding values from Ref. 45 of 85%, 11%, and 0%.

Visualization of coordination environments[65] reveals the mechanism by which fivefold coordination states are formed at low compression (Fig. 5). The mechanism is a momentary closing of the Si-O-Si angle between two tetrahedra, which brings a fifth oxygen within the coordination shell of one of the Si atoms. The product is a shared edge between a pentrahedron and a tetrahedron and one three-coordinated oxygen. The Si-Si coordination number is unchanged by this process as is the network connectivity: no new connections are formed between coordination environments. At higher compression, not only higher coordination numbers but also edge sharing is much more common. At V3T3, a wide variety of coordination environments and shared elements are present, while a significant amount of free volume remains between the coordination polyhedra. Finally, at V4T4, the structure begins to resemble a close-packing arrangement, with little free volume, and common face sharing as well as edge sharing and little corner sharing.

We now examine the distributions of the O-Si-O and Si-O-Si bond angles in liquid silica (Fig. 6). The average angles of O-Si-O distributions at V1T1 and V2T2 are 108.4° and 107.6°, respectively, in agreement with the previous FPMD study[43] and close to the ideal tetrahedral angle (109.47°) found with small deviations in the tetrahedral crystalline polymorphs and silica glass at ambient conditions. With increasing temperature, the distribution becomes broader with its average value slightly shifting to smaller angles (Fig. 6, top). On compression beyond $V/V_X=0.7$, the distribution becomes bimodal; at V4T4, the two modes are centered at 87° and 137° and become narrower with decreasing temperature. The first peak represents the characteristic octahedral angle of 90°, whereas the second peak represents the angle made by two opposite O atoms with the center Si atom. The distribution of the Si-O-Si bond angle shows a single broad peak at all conditions (Fig. 6, bottom). With increasing temperature, the distribution broadens, and the small-angle tail extends to smaller angles. On compression, the distribution becomes sharper and more asymmetric with the peak and small-angle tail shifts to smaller angles. The average values of the distribution at V1T1 and V2T2 are 133.5° and 126.8°, compared to an angle of 144° for the glass at 300 K.[23] The distribution extending below 120° down to angles as small as 70° contains contributions from edge-sharing polyhedra. At conditions V3T3 and V4T4, the average values of the distribution are 114.9° and 110.8°, as expected of edge- and face-sharing polyhedra.

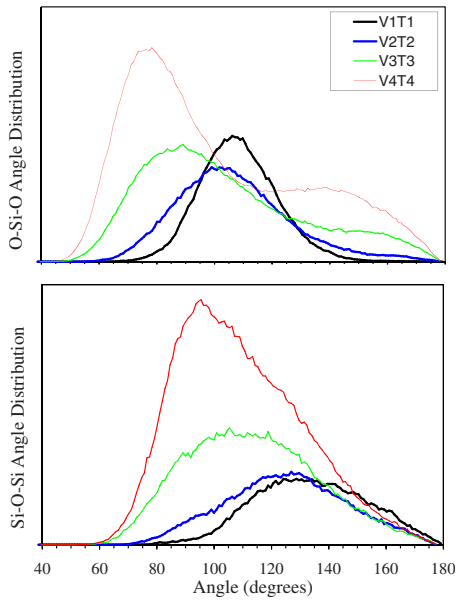

FIG. 6. (Color online) O-Si-O (top) and Si-O-Si (bottom) bond-angle distributions in liquid silica at conditions V1T1, V2T2, V3T3, and V4T4.

The initial compression mechanisms in silica liquid from $V/V_X=1.0$ to 0.8 cannot be understood on the basis of the local structural features explored so far. The coordination increase is slight over this range, and nearest neighbor bond distances increase with compression. It has been suggested that changes in intermediate range order in the form of ring statistics can account for the initial compression of silica liquid based on simulations using a semiempirical force field.[66] In particular, it was argued that a decrease in the number of small rings and an increase in the characteristic ring size are of the primary compression mechanisms. In order to test this idea, we compute the ring statistics in our simulations. Our results show an initial decrease in the proportions of 3-rings with compression (Fig. 7, top). Moreover, the characteristic ring size calculated by using the approach of Ref. 67 increases on compression (Fig. 7, bottom). The number of small rings increases upon further compression ($V/V_X \leqslant 0.7$) due to the increase in Si-O coordination number, a feature absent from the previous simulations,[66] which used a semiempirical potential model that forced fourfold coordination to be maintained. We also find a small proportion of 2-rings, which are not included in the analysis of the

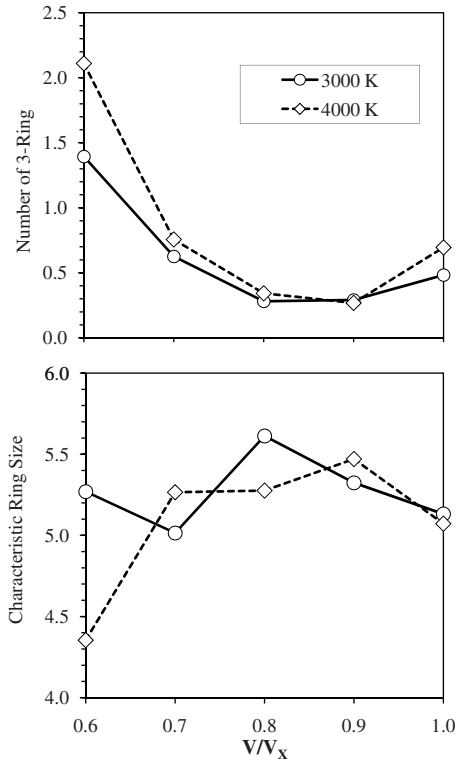

FIG. 7. Ring statistics of liquid silica: The number of 3-ring (top) and characteristic ring size (bottom) at 3000 and 4000 K.

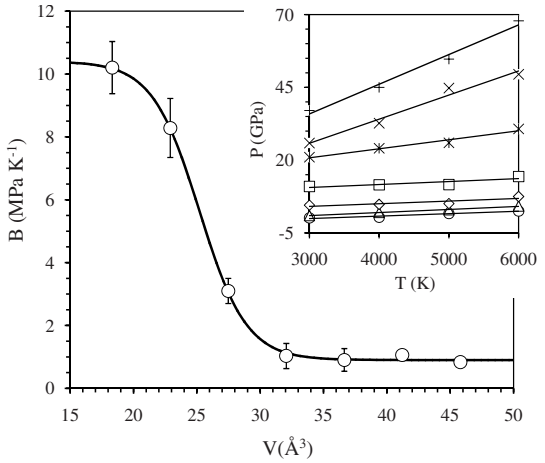

FIG. 8. Volume dependence of thermal pressure coefficient B defined by Eq. (5) in the text. The symbols represent the calculated temperature derivatives of the pressure at different volumes obtained from linear fit to the temperature variation of the total pressure shown in the inset. The symbols in the inset represent the calculated results at $V/V_X=1.0$ (circles), 0.9 (diamonds), 0.8 (triangles), 0.7 (squares), 0.6 (asterisks), 0.5 (crosses), and 0.4 (pluses). Errors are within the size of the symbols. Lines represent the linear fits. For the sake of convenience, pressures at $V/V_X=0.5$ and 0.4 are shifted by −15 and −90 GPa (i.e., downward), respectively.

characteristic ring size. These are primarily associated with the formation of fivefold coordinated Si, by the mechanism discussed above, and so do not influence the network connectivity. Our results are at odds with those of a previous FPMD study[45] that found the number of 3-rings increasing on compression. The origin of this discrepancy is unclear, but may be due to longer run duration of our simulations.

B. Equations of state

The calculated pressure-volume-temperature results are described with the Mie-Grüneisen equation of state,

$$P(V,T) = P(V,T_0) + P_{\text{th}}(V,T), \tag{3}$$

where $P(V,T_0)$ is the pressure on the reference isotherm, $T=T_0$, and $P_{\text{th}}(V,T)$ is the thermal pressure. As shown in the inset of Fig. 8, the thermal pressure increases nearly linearly with temperature at all volumes. The increase of thermal pressure on compression is initially gradual and then becomes more rapid at $V/V_X \geqslant 0.7$. The thermal pressure is represented by

$$P_{\text{th}}(V,T) = B(V)(T - T_0), \tag{4}$$

where the thermal pressure coefficient B may be represented over the range of our simulations by

$$B(V) = 10.4 - \frac{9.5}{1 + \exp[(25.2 - V)/1.86]}, \tag{5}$$

in units of MPa K^{-1} (Fig. 8). The reference isotherm, taken to be $T_0=3000$ K, is described by the fifth order Birch-Murnaghan equation of state with zero pressure, volume, bulk modulus, and first and second pressure derivatives of the bulk modulus: $V_0=45.8$ (±0.2) Å^3/SiO_2, $K_0=5.2$ (±1) GPa, $K_0'=22.5$ (±3), and $K_0K_0''=-452.3$ (±24). The necessity of using such a high order fit further illustrates the differences in compression mechanisms already discussed between silica liquid and $MgSiO_3$ liquid, which requires only a third order fit. The calculated P-V isotherms initially remain close and nearly parallel to each other on compression, and then begin to diverge on further compression beyond $V/V_X=0.7$ (Fig. 9). For comparison, we also perform simulations of the crystalline phases quartz, stishovite, and seifertite (alpha-PbO_2 structure) at 3000 K.[68–72] By comparing the slope of the equation of state in pressure-volume space, we see that the liquid phase is more compressible than any of the solid phases when compared at the same volume. The density of the liquid exceeds that of quartz at a pressure of about 4 GPa, consistent with previous experimental[73] and theoretical analyses.[45] At 3000 K, the density of the liquid also exceeds that of stishovite at about 90 GPa and seifertite at approximately 120 GPa. These liquid-crystal density inversions are consistent with a recent analysis of the high-pressure melting curve of silica, which finds vanishing dT_M/dP melting slopes at similar pressures.[59] A complete analysis of the melting curve is beyond the scope of this study.

Our results agree well with experimental determinations of the equation of state of liquid SiO_2. At low pressure, various experimental analyses[18–22] have yielded significantly different results, which span our predicted equation of state (inset of Fig. 9). Our results are in excellent agreement with high-pressure high-temperature shock-wave data.[59] Our cal-

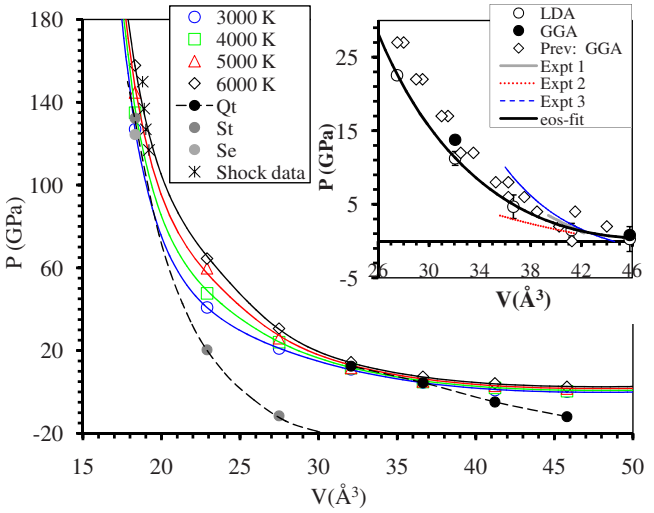

FIG. 9. (Color online) Equation of state of silica liquid: Lines are the Mie-Grüneisen fits to the calculated pressure-volume results shown by open circles (3000 K), squares (4000 K), triangles (5000 K), and diamonds (6000 K). Errors are within the size of the symbols. The dashed lines show the equation of state for the solid phases along 3000 K isotherm (Qt, quartz; St, stishovite; Se, seifertite). The shock-compression data (red asterisks at 4900 and 5320 K and black asterisks at 5760 and 6500 K) for silica melt are from Ref. 59. Inset: Comparison of our results at 3500 K with previous GGA results at 3500 K (Ref. 45) and with the experimental results (Expt 1 from Ref. 18, Expt 2 from Refs. 18 and 20, and Expt 3 from Ref. 22) at 1623 K. The uncertainties for liquid at 3500 K are based on the averages taken between results at 3000 and 4000 K.

culated pressure for density of 4.71 g/cm^3 at 8000 K is 106.5 GPa, compared with the value from a previous FPMD simulation of 110 GPa.[74] Our GGA simulations agree well with previous GGA results[45] (inset of Fig. 9).

We calculate the thermal Grüneisen parameter, defined as $\gamma=(V/C_V)(\partial P_{\rm th}/\partial T)$, where $C_V=\partial E/\partial T$ is the heat capacity at constant volume. As in the case of the thermal pressure, a linear equation is fitted to the calculated energy-temperature results at each volume (inset of Fig. 10). Our results show that C_V and γ tend to decrease and increase, respectively, with compression in a nonlinear way (Fig. 10). Two distinct regions appear: a low-compression region characterized by little variation with compression and large and small values of C_V and γ, respectively, and a high-compression region characterized by more rapid variations with volume and by small C_V and large γ. The heat capacity of the silica liquid substantially exceeds the Dulong-Petit value. Our results for C_V are larger than previous MD results,[11] and both sets of theoretical results are larger than the experimental values.[75] The reason for the difference between theory and experiment in this case is not clear. It should be noted that our previous first-principles molecular dynamics simulations of $MgSiO_3$ liquid are in excellent agreement with experimental heat capacity data.[14] It is possible that the heat capacity depends strongly on temperature at temperatures below the range of our study, although this seems unlikely based on the linearity of the energy-temperature relation.

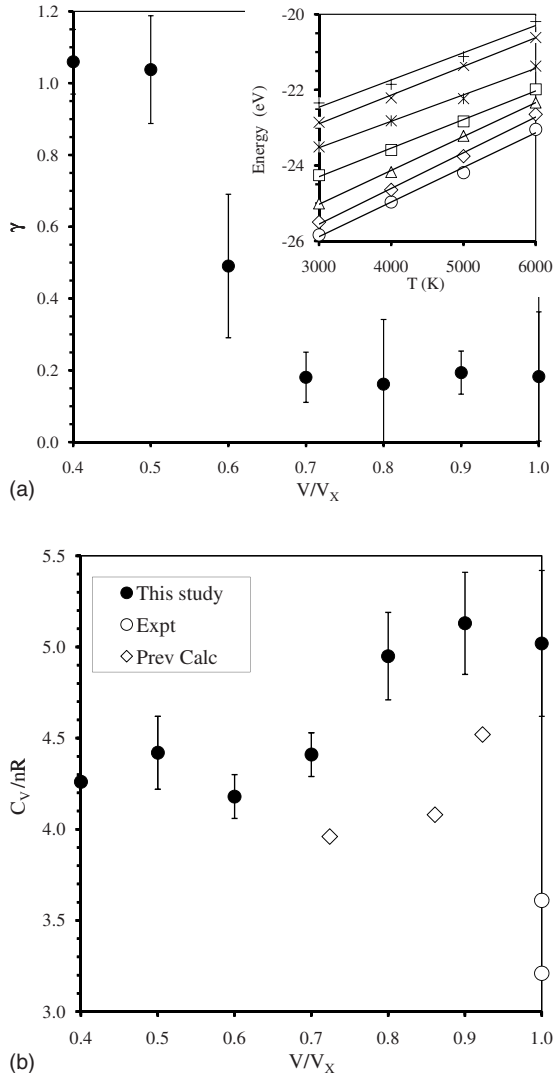

FIG. 10. Calculated temperature-averaged Grüneisen parameter and heat capacity as a function of compression. Previous MD results (averaged between 3000 and 6000 K) (Ref. 11) and experimental data (Ref. 59) for C_V are shown. The inset shows the temperature variations of the total energy at different volumes: V/V_X =1.0 (circles), 0.9 (diamonds), 0.8 (triangles), 0.7 (squares), 0.6 (asterisks), 0.5 (crosses), and 0.4 (pluses). Errors are within the size of the symbols. Lines represent the linear fits. For the sake of convenience, energies at V/V_X=1.0, 0.9, 0.8, 0.7, 0.6, 0.5, and 0.4 are shifted by −1.5, −1.0, −0.5, 0.0, 0.5, 1.0, and 0.0 eV, respectively.

C. Dynamical properties

We compute the self-diffusion coefficient as

$$D=\lim_{t\to\infty}\frac{\langle[r(t)]^2\rangle}{6t}, \tag{6}$$

where

$$\langle[r(t)]^2\rangle=\frac{1}{N}\sum_{i=1}^{N}|r_i(t)-r_i(0)|^2 \tag{7}$$

is the MSD and $r_i(t)$ is the position of the ith atom at time t (Figs. 11 and 12). The partial MSD is then calculated by

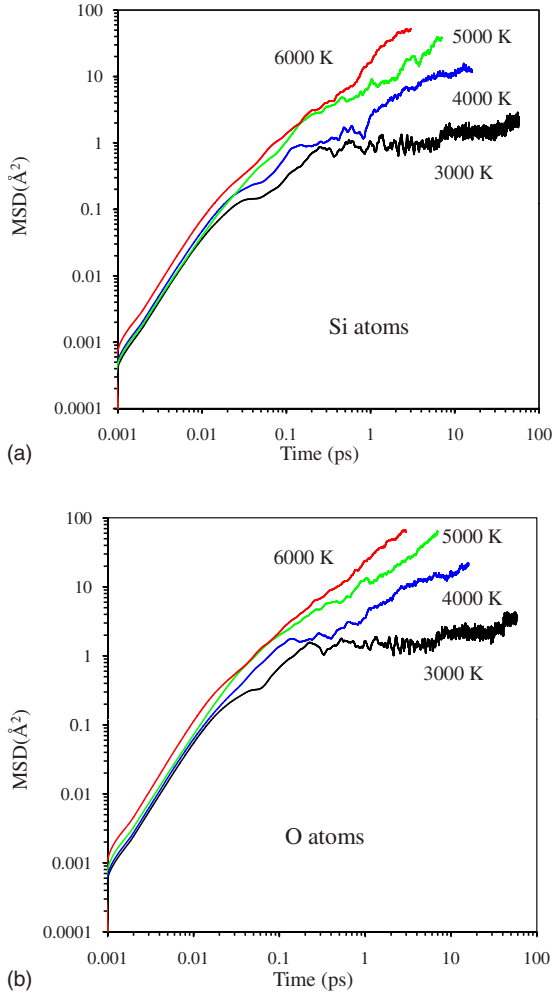

FIG. 11. (Color online) Mean-square displacement (MSD) versus time relationships for Si and O atoms at $V/V_X=1.0$ for four different temperatures: 3000, 4000, 5000, and 6000 K (from lower to upper curves).

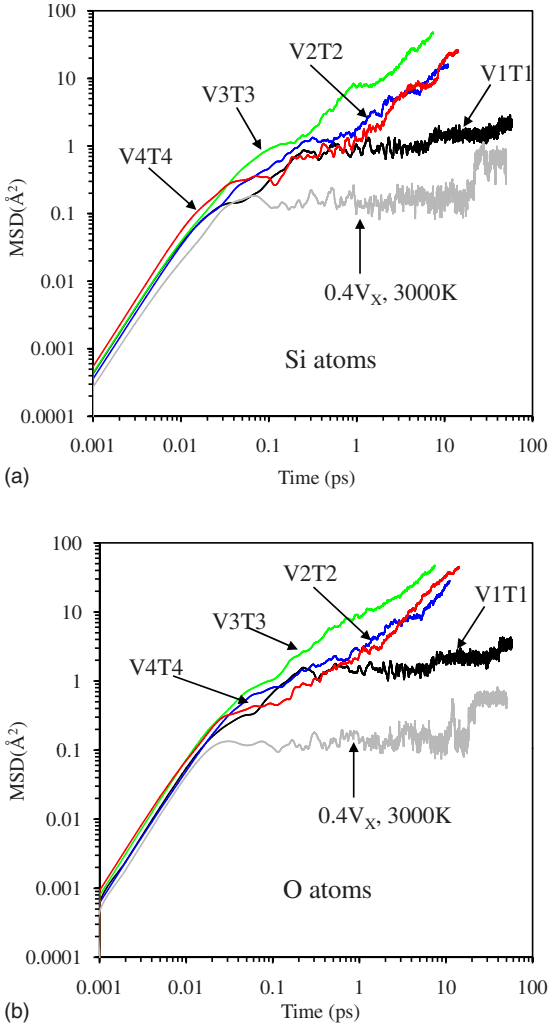

FIG. 12. (Color online) Mean-square displacement (MSD) versus time relationships for Si and O atoms at four different compression-temperature conditions: V1T1, V2T2, V3T3, and V4T4. The lowermost curve in each plot is MSD at 3000 K for the smallest volume ($V/V_X=0.4$).

averaging over atoms of a given species. We account for the translational symmetry of the system so that the MSD value is not restricted by the size of the supercell. At high temperatures of 5000 and 6000 K, each MSD clearly shows two temporal regimes. The first is the ballistic regime (for short times) in which the atoms move without interacting strongly with their neighbors and MSD is proportional to t^2. The second is the diffusion regime (for long times) in which MSD is proportional to t. However, at 3000 and 4000 K, an intermediate regime appears where MSD increases slowly due to the so-called cage effect. The atoms are temporarily trapped in the cages made by their neighbors. The duration of the cage regime increases rapidly with decreasing temperature spanning 0.1–1 ps at 4000 K and 0.2–20 ps at 3000 K. This is consistent with a previous FPMD study.[46] At 3000 K, the curves show additional features; immediately after the ballistic regime, the curves show a small shoulder at around 0.03 ps and a peak at around 0.2 ps. As suggested previously,[40] the first feature can be associated with the complex local motion of the atoms in the open tetrahedral network and the second with the so-called boson peak related to a low-frequency vibrational mode.

The calculated diffusion coefficient at the reference volume ($V=V_X$) as a function of the inverse temperature follows the Arrhenius relation (Fig. 13). Our analysis is made at constant volume (along $V/V_X=1.0$ isochore), and the corrections to constant pressure are within uncertainties. The calculated activation energies are 3.43(8) and 3.27(12) eV for silicon and oxygen, respectively. These numbers are relatively small, compared to the experimental values for vitreous silica at lower temperatures of 6.0 and 4.7 eV, respectively, for Si (Ref. 31) and O (Ref. 32), and a more recent experimental value of 4.74 eV for Si diffusion.[33] The difference between our results and experiment may be explained by a crossover from strong Arrhenian behavior at the low temperatures of the experiments to fragile, non-Arrhenian behavior within the temperature range of our simulations.[40] Previous MD studies based on semiempirical interatomic force models have produced a wide range of activation energies as the predicted diffusion constants differ by up to two decades.[40,41,77,78] Our results are slightly smaller than those

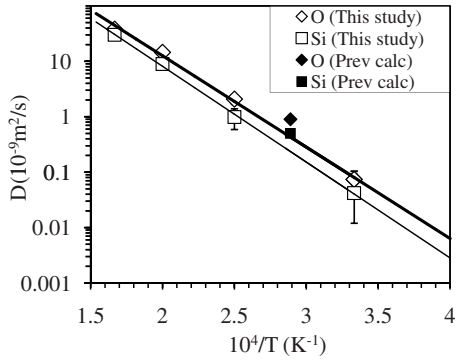

FIG. 13. Calculated diffusion coefficients (symbols) for Si and O atoms as a function of temperature at $V/V_X=1.0$. Lines represent the fit to the Arrhenius law. Previous calculated values are from Ref. 44.

from a previous FPMD study;[43] the small difference may be due to the greater duration of our simulations. A crossover to fragile behavior at high temperature would suggest nonlinear dependence of the diffusion coefficient on inverse temperature over the range of our simulations. Indeed, we cannot rule out a nonlinear dependence within our uncertainties, in which case the values quoted above for the activation energies should be considered as average values over the temperature range of our simulations.

Very long simulations at compressed volumes are needed for 3000 K (the lowest temperature studied) to obtain the fully converged diffusion coefficients. For instance, at the smallest volume ($V/V_X=0.4$) used, the 3000 K MSD remains below 0.9 Å^2 over the run of about 60 ps (Fig. 12). This behavior is consistent with a vitreous (nondiffusional) state. We calculate the diffusion coefficients only at those volume-temperature points where we see a clear evidence for the beginning of the diffusional regime. At 4000 K, with increasing pressure, the calculated diffusion coefficient initially increases, reaching a maximum at approximately 25 GPa, and then decreases with further increase in pressure (Fig. 14). A similar maximum is weakly present at 5000 K and absent at 6000 K, where the diffusion coefficient decreases monotonically with increasing pressure to within our uncertainty. Previous MD studies have also predicted diffusivity maxima at temperatures ranging from 3000 to 5000 K.[11,13,38,41,77–79] The Arrhenius law cannot represent the complete set of calculated pressure-temperature values of diffusivity of silica liquid due to the diffusivity maximum. We include only those pressure-temperature points in the Arrhenius analysis which show a diffusivity decreasing with increasing pressure including all seven volumes at 6000 K, $V/V_X \leqslant 0.9$ at 5000 K, and $V/V_X \leqslant 0.6$ at 4000 K. Thus derived activation energy and activation volume for the total diffusivity are 2.0 eV and 1.2 Å^3, respectively. The activation energy is substantially less than that (3.35 eV) at $V/V_X=1.0$, which emphasizes difference in diffusional behavior in silica liquid between low and high pressures. For comparison, the corresponding values for MgO from the Arrhenius fit to a complete set of P and T results for the total diffusivity are 0.83 eV and 1.3 Å^3, respectively.[49] We note that the apparently Arrhenian regime that we have

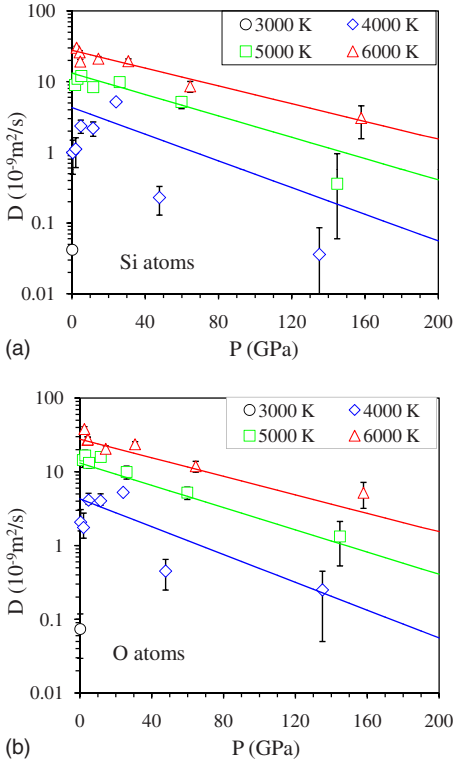

FIG. 14. (Color online) The calculated diffusion coefficients for Si and O atoms as a function of pressure at four temperatures: 3000 K (circles), 4000 K (diamonds), 5000 K (squares), and 6000 K (triangles). The lines are Arrhenius fit to the selected data points (see the text).

analyzed is geophysically relevant as it encompasses pressure-temperature conditions at which partial melting would be expected in Earth's mantle.

Previous MD studies have shown that finite-size effects on diffusivity of silica liquid can be substantial.[38,79,80] The diffusion coefficient at zero pressure varies with the number (N) of atoms as $1/N$ at 3000 K or as $1/N^{1/3}$ at 6000 K.[80] We estimate, based on these results, that our simulations may underestimate the diffusion coefficient by 20% at 6000 K and by 45% at 3000 K, relative to the infinite system limit. Since the finite-size effect is systematic, we may estimate the value of the zero-pressure activation energies in infinite system limit: 3.22 and 3.19 eV, respectively, for Si and O, i.e., a few percent difference. Finite-size scaling is not well known at high pressure, although little difference between systems with 324 and 728 atoms was previously found by MD simulation.[79] We note that the height of our diffusivity maximum at 4000 K is about 3.5×10^{-9} m^2/s relative to the value at $V/V_X=1.0$, which is much larger than the potential finite-size errors.

IV. DISCUSSION AND CONCLUSIONS

Liquid silica has been predicted to display several anomalies, including a temperature of maximum density (TMD), spinodal instability, and liquid-liquid phase transformations[9–11] that so far have not been studied with

first-principles methods. Predictions of these anomalies have been based on semiempirical interatomic force models, including van Beest–Kramer–van Santen (BKS)[76] and Woodcock-Angell-Cheeseman (WAC).[77] The prediction of a TMD has led several authors to draw analogies between the behavior of silica and water.[3] More recent studies have shown that the dependence of TMD on volume and the magnitude of negative thermal expansivity are sensitive to the assumed form of the atomic interactions.[9,10]

Our results show no evidence for a TMD. In particular, the pressure increases monotonically and nearly linearly with increasing temperature along all isochores investigated (Fig. 8). This is in contrast to the strongly concave dependence of pressure with temperature along isochores found in previous results based on semiempirical potentials.[9] For example, at a density of 2.2 g/cm^3, similar to our $V/V_X=1.0$, Ref. 9 finds that the pressure decreases with increasing temperature up to a temperature of 9000 K, where the pressure is 10 GPa less than that at 3000 K according to the WAC model. The magnitude of this local pressure minimum lies well outside the uncertainties of our simulations. The BKS model produces more subtle effects (pressure at 5000 K is 4 GPa less than that at 2500 K), which can nevertheless also be excluded by our simulations.

We find no evidence of spinodal instabilities (vanishing bulk modulus) over the range of our first-principles simulations. The pressure monotonically increases with decreasing volume along all isotherms (Fig. 9). Spinodals have been found in previous simulations of liquid silica, behavior that has been connected to the possibility of liquid-liquid phase transformations.[9–11] The WAC potential predicts two spinodals on the 3000 K isotherm at 8 and 10 GPa, whereas the BKS potential predicts spinodals at positive pressure for $T>6500$ K and $T<2000$ K,[9] outside the range of our results. We cannot rule out the presence of spinodal instabilities outside the range of our results. Indeed, extrapolation of our equation of state fit at 3000 K shows a spinodal at a pressure of −0.12 GPa and $V/V_X=1.05$. Our results show no signs of spinodal instability at temperatures higher than the range investigated here on the basis of the nearly linear dependence of pressure on temperature.

The disagreement between pair potentials and first-principles simulations calls into question the accuracy of the pair potentials. Even if two quite different pair potentials yield qualitatively similar results, it does not necessarily follow that the qualitative trends are realistic. This may be because of the limitations in the functional form of the pair potentials: the well-known Born-Mayer form[81] may not capture the essential physics of bonding.[42] Indeed, by including polarizability, Ref. 82 finds much better agreement with first-principles simulations of liquid silica.

We find that silica liquid is characterized by two distinct compressional regimes: a low-pressure regime ($V/V_X>0.7$) in which the Si-O coordination number is nearly constant and a high-pressure regime ($V/V_X\leqslant 0.7$) in which the Si-O coordination number increases relatively rapidly. These two regimes are characterized by distinct thermodynamic properties. In the low-pressure regime, the liquid is much more compressible, the heat capacity is higher, and the Grüneisen parameter is smaller than in the high-pressure regime. The behavior of silica liquid is thus quite distinct from $MgSiO_3$ liquid in which the Si-O coordination number and the Grüneisen parameter depend essentially linearly on compression.

Structural compression mechanisms in these two regimes are fundamentally different. In the high-pressure regime, compression is primarily associated with an increase in the Si-O coordination number. The low-pressure regime displays a unique compression mechanism that is not seen in any crystalline silicate. Whereas crystalline silicates compress either by decreasing nearest neighbor bond lengths (e.g., stishovite) or the distances (angles) between coordination polyhedra (e.g., quartz or coesite), neither of these two compression mechanisms occur in the liquid. Instead, the liquid compresses by altering its medium range structure as manifested in the ring statistics.[66] In particular, the number of small rings decreases with compression, and the ring size increases. These results are understood in terms of the relative pruning efficiency of different sized rings as they are formed in a Bethe lattice, and rationalized by comparison with a suite of crystalline silicate structures, which show a wide variety of ring statistics and a range of framework densities over a factor of 3, with the least dense frameworks associated with the largest number of small rings.[67] The topological compression mechanism found in silica liquid is potentially very important for understanding the behavior of polymerized silicate liquids at elevated pressure. The reason is that the topological mechanism is operative in the pressure regime where the liquid is most compressible, and therefore is responsible for a large fraction of the compression over the pressure regime of Earth's mantle.

An alternative interpretation of compression in the low-pressure regime was offered by Trave *et al.*[45] They argued that increased network connectivity due to the presence of a small fraction of fivefold coordinated Si is primarily responsible for compression in this regime. While this may also be a contributing factor, it is not clear how this mechanism can lead to substantial amounts of compression. Unlike the ring-growth mechanism discussed above, it is not possible to use crystalline models to quantify the relationship between the compression mechanism and density. Moreover, we find that formation of fivefold coordination Si does not increase network connectivity, at least at low pressure.

The dynamical properties of silica liquid are also found to show two distinct regimes, a low-compression anomalous regime showing a temperature-dependent diffusivity maximum and a high-compression regime in which the diffusion coefficient decreases with increasing pressure. We find that the diffusivity maximum is closely associated with the presence of fivefold coordinated Si, in agreement with previous studies.[41] The pentahedral coordination environments can be considered as transition states for atomic diffusion. In particular, the pressure at which fivefold coordinated Si is most abundant coincides with the pressure of the diffusivity maximum at 4000 K. We confirm from first principles the diffusivity maximum in silica liquid, which was previously predicted by MD simulations based on interatomic force models.[13,38,41,78,79] A clear pattern in our results has not been widely discussed: the vanishing of the diffusivity maximum with increasing temperature. Indeed, the strong temperature dependence is at odds with a previous explanation of the

diffusivity maximum as being associated with the crystalline fourfold to sixfold coordination change.[79] This model would predict that the diffusivity maximum should either be independent of temperature or move to higher pressures with increasing temperature, contrary to our findings. Our results are consistent with a picture in which silica liquid behaves like a strong liquid at low pressure and low temperature and a fragile liquid at high pressure and high temperature. This explains the diffusivity maximum, its temperature dependence, and the difference between the high-temperature activation energy obtained from our simulations and the larger, lower-temperature activation energy found in experiments.

ACKNOWLEDGMENTS

This work was supported by the NSF Grants No. EAR-0409074 (B.B.K.) and No. EAR-048182 (L.S.). Computing facilities were provided by CCT at Louisiana State University.

[1] C. A. Angell and H. Kanno, Science **193**, 1121 (1976).
[2] F. X. Prielmeier, E. W. Lang, R. J. Speedy, and H.-D. Lüdemann, Phys. Rev. Lett. **59**, 1128 (1987).
[3] P. H. Poole, M. Hemmati, and C. A. Angell, Phys. Rev. Lett. **79**, 2281 (1997).
[4] O. Mishima and H. E. Stanley, Nature (London) **396**, 329 (1998).
[5] M. Hemmati, C. T. Moynihan, and C. A. Angell, J. Chem. Phys. **115**, 6663 (2001).
[6] J. C. Phillips, J. Non-Cryst. Solids **34**, 153 (1979).
[7] W. A. Crichton, M. Mezouar, T. Grande, S. Stolen, and A. Grzechnik, Nature (London) **414**, 622 (2001).
[8] C. A. Angell, R. D. Bressel, M. Hemmati, E. J. Sare, and J. C. Tuker, Phys. Chem. Chem. Phys. **2**, 1559 (2000).
[9] I. Saika-Voivod, F. Sciortino, and P. H. Poole, Phys. Rev. E **63**, 011202 (2000).
[10] I. Saika-Voivod, P. H. Poole, and F. Sciortino, Nature (London) **412**, 514 (2001).
[11] S. R. Ren, I. W. Hamley, P. I. C. Teixeira, and P. D. Olmsted, Phys. Rev. E **63**, 041503 (2001).
[12] S. Stolen, T. Grande, and H. B. Johnsen, Phys. Chem. Chem. Phys. **4**, 3396 (2002).
[13] R. Sharma, A. Mudi, and C. Chakravarty, J. Chem. Phys. **125**, 044705 (2006).
[14] L. Stixrude and B. B. Karki, Science **310**, 297 (2005).
[15] Q. Williams and J. Garnero, Science **273**, 1528 (1996).
[16] E. Stolper, D. Walker, B. H. Hager, and J. F. Hays, J. Geophys. Res. **86**, 6261 (1981).
[17] G. H. Miller, E. M. Stolper, and T. J. Ahrens, J. Geophys. Res. **96**, 11849 (1991).
[18] G. A. Gaetani, P. D. Asimow, and E. M. Stolper, Geochim. Cosmochim. Acta **62**, 2499 (1998).
[19] J. Zhang, R. C. Liebermann, T. Gasparik, and C. T. Herzberg, J. Geophys. Res. **98**, 19785 (1993).
[20] R. A. Lange and I. S. E. Carmichael, Geochim. Cosmochim. Acta **51**, 2931 (1987).
[21] V. C. Kress and I. S. E. Carmichael, Contrib. Mineral. Petrol. **108**, 82 (1991).
[22] P. Hudon, I. H. Jung, and D. R. Baker, Phys. Earth Planet. Inter. **130**, 159 (2002).
[23] R. L. Mozzi and B. E. Warren, J. Appl. Crystallogr. **2**, 164 (1969).
[24] R. J. Hemley, H. K. Mao, P. M. Bell, and B. O. Mysen, Phys. Rev. Lett. **57**, 747 (1986).
[25] D. L. Price and J. M. Carpenter, J. Non-Cryst. Solids **92**, 153 (1987).
[26] Q. Williams and R. Jeanloz, Science **239**, 902 (1988).
[27] P. A. V. Johnson, A. C. Wright, and R. N. Sinclair, J. Non-Cryst. Solids **58**, 109 (1990).
[28] X. Xue, J. F. Stebbins, M. Kanzaki, P. F. McMillan, and B. Poe, Am. Mineral. **76**, 8 (1991).
[29] S. Susman, K. J. Volin, D. L. Price, M. Grimsditch, J. P. Rino, R. K. Kalia, P. Vashishta, G. Gwanmesia, Y. Wang, and R. C. Liebermann, Phys. Rev. B **43**, 1194 (1991).
[30] C. Meade, R. J. Hemley, and H. K. Mao, Phys. Rev. Lett. **69**, 1387 (1992).
[31] G. Brebec, R. Sefuin, C. Sella, J. Bevenot, and J. C. Martin, Acta Metall. **28**, 327 (1980).
[32] J. C. Mikkelsen, Appl. Phys. Lett. **45**, 1187 (1984).
[33] D. Tsoukalas, C. Tsamis, and P. Normand, J. Appl. Phys. **89**, 7809 (2006).
[34] J. R. Rustad, D. A. Yuen, and F. J. Spera, Phys. Rev. B **44**, 2108 (1991); Chem. Geol. **96**, 421 (1992).
[35] L. Stixrude and M. S. T. Bukowinski, Phys. Rev. B **44**, 2523 (1991).
[36] J. P. Rino, I. Ebbsjo, R. K. Kalia, A. Nakano, and P. Vashishta, Phys. Rev. B **47**, 3053 (1993).
[37] W. Jin, R. K. Kalia, P. Vashishta, and J. P. Rino, Phys. Rev. Lett. **71**, 3146 (1993).
[38] J. R. Rustad, D. A. Yuen, and F. J. Spera, Phys. Rev. A **42**, 2081 (1990).
[39] C. S. Marians and L. W. Hobbs, J. Non-Cryst. Solids **124**, 242 (1990).
[40] J. Horbach and W. Kob, Phys. Rev. B **60**, 3169 (1999).
[41] C. A. Angell, P. A. Cheeseman, and S. Tamaddon, Science **218**, 885 (1982).
[42] L. Stixrude, in *Structure and Imperfections in Amorphous and Crystalline Silicon Dioxide*, edited by R. A. B. Devine, J.-P. Duraud, and E. Dooryhée (Wiley, New York, 2000), pp. 69–103.
[43] J. Sarnthein, A. Pasquarello, and R. Car, Phys. Rev. Lett. **74**, 4682 (1995).
[44] J. Sarnthein, A. Pasquarello, and R. Car, Phys. Rev. B **52**, 12690 (1995).
[45] A. Trave, P. Tangney, S. Scandolo, A. Pasquarello, and R. Car, Phys. Rev. Lett. **89**, 245504 (2002).
[46] M. Pohlmann, M. Benoit, and W. Kob, Phys. Rev. B **70**, 184209 (2004).
[47] G. Kresse, J. Hafner, and R. J. Needs, J. Phys.: Condens. Matter **4**, 7451 (1992).
[48] G. Kresse and J. Furthmuller, Comput. Mater. Sci. **6**, 15 (1996).
[49] B. B. Karki, D. Bhattarai, and L. Stixrude, Phys. Rev. B **73**,

174208 (2006).
[50] B. B. Karki, D. Bhattarai, and L. Stixrude, Comput., Mater., Continua **3**, 107 (2006).
[51] N. D. Mermin, Phys. Rev. **137**, A1441 (1965); A. K. Mcmahan and M. Ross, Phys. Rev. B **15**, 718 (1977).
[52] D. M. Ceperley and B. J. Alder, Phys. Rev. Lett. **45**, 566 (1980).
[53] B. B. Karki, L. Stixrude, and R. M. Wentzcovitch, Rev. Geophys. **39**, 507 (2001).
[54] Y. Wang and J. P. Perdew, Phys. Rev. B **44**, 13298 (1991).
[55] G. P. Francis and M. C. Payne, J. Phys.: Condens. Matter **2**, 4395 (1990).
[56] A. R. Oganov, J. P. Brodholt, and G. D. Price, Nature (London) **411**, 934 (2001).
[57] R. M. Wentzcovitch, B. B. Karki, M. Cococcioni, and S. de Gironcoli, Phys. Rev. Lett. **92**, 018501 (2004).
[58] M. J. Allen and D. J. Tildesley, *Computer Simulation of Liquids* (Oxford University Press, Oxford, 1987).
[59] J. A. Akins and T. J. Ahrens, Geophys. Res. Lett. **29**, 1394 (2002).
[60] H. Flyvbjerg and H. G. Petersen, J. Chem. Phys. **91**, 461 (1989).
[61] Y. Waseda and J. M. Toguri, Metall. Trans. B **8**, 563 (1977).
[62] G. H. Wolf, D. J. Durben, and P. F. McMillan, J. Chem. Phys. **93**, 2280 (1990).
[63] D. L. Farber and Q. Williams, Am. Mineral. **81**, 273 (1996).
[64] J. F. Stebbins, I. S. E. Carmichael, and L. K. Moret, Contrib. Mineral. Petrol. **86**, 131 (1984).
[65] D. Bhattarai and B. B. Karki, The 14th International Conference on Central Europe in Computer Graphics, Visualization and Computer Vision (WSCG'06), 2006, pp. 17–24; D. Bhattarai, B. B. Karki, and L. Stixrude, Visual Geosci. **11**, 1 (2006).
[66] L. Stixrude and M. S. T. Bukowinski, Science **250**, 541 (1990).
[67] L. Stixrude and M. S. T. Bukowinski, Am. Mineral. **75**, 1159 (1990).
[68] D. R. Hamann, Phys. Rev. Lett. **76**, 660 (1996).
[69] B. B. Karki, M. C. Warren, L. Stixrude, G. J. Ackland, and J. Crain, Phys. Rev. B **55**, 3465 (1997); **56**, 2884(E) (1997).
[70] A. R. Oganov, M. J. Gillan, and G. D. Price, Phys. Rev. B **71**, 064104 (2005).
[71] I. Saika-Voivod, F. Sciortino, T. Grande, and P. H. Poole, Phys. Rev. E **70**, 061507 (2004).
[72] I. Saika-Voivod, F. Sciortino, T. Grande, and P. H. Poole, Philos. Trans. R. Soc. London, Ser. A **383**, 525 (2004).
[73] R. J. Hemley, A. P. Jephcoat, H. K. Mao, L. C. Ming, and M. H. Manghnani, Nature (London) **334**, 52 (1988).
[74] Y. Laudernet, J. Clérouin, and S. Mazevet, Phys. Rev. B **70**, 165108 (2004).
[75] P. Richet, Y. Bottinga, L. Denielou, J. P. Petitet, and C. Tequi, Geochim. Cosmochim. Acta **46**, 2639 (1982).
[76] B. W. H. van Beest, G. J. Kramer, and R. A. van Santen, Phys. Rev. Lett. **64**, 1955 (1990).
[77] L. V. Woodcock, C. A. Angell, and P. A. Cheeseman, J. Chem. Phys. **65**, 1565 (1976).
[78] S. K. Mitra, Philos. Mag. B **45**, 529 (1982).
[79] S. Tsuneyuki and Y. Matsui, Phys. Rev. Lett. **74**, 3197 (1995).
[80] G. Zhang, G. Guo, K. Refson, and Y. Zhao, J. Phys.: Condens. Matter **16**, 9127 (2004).
[81] N. H. March and M. P. Tosi, *Coulomb Liquids* (Academic, New York, 1984).
[82] P. Tangney and S. Scandolo, J. Chem. Phys. **117**, 8898 (2002).